Observation of Proton Transfer in 2-Aminopyridine Dimer by Electron and Mass Spectroscopy

Elena Samoylova, Wolfgang Radloff, Hans-Hermann Ritze, and Thomas Schultz*

Max-Born-Institute, Max-Born-Str. 2A, 12489 Berlin, Germany

Received: April 15, 2009; Revised Manuscript Received: May 29, 2009

A photoinitiated intermolecular electron−proton transfer reaction in 2-aminopyridine dimer was investigated by femtosecond pump−probe electron−ion coincidence spectroscopy and accompanying theory. Excited-state population dynamics were observed in real time by time-resolved mass spectroscopy, and the respective excited-state character of locally excited and proton/hydrogen transfer states was identified in coincident electron spectra. Two reaction channels for an ultrafast (sub-50 fs) and a slower (∼75 ps) proton/hydrogen transfer were observed and indicate that vibrational energy redistribution may lead to efficient population trapping in the excited state. Spectroscopic evidence of an unexpected hydrogen-transfer reaction in photoexcited aminopyridine monomer is also presented.

I. Introduction

Ab initio theory can identify photochemical reaction coordinates in small molecular systems but must make assumptions about the relevant electronic and nuclear degrees of freedom to address larger systems. Comparison with experimental data is therefore crucial to characterize photoinitiated processes in molecular systems. Time-resolved photoelectron spectroscopy (TRPES) is particularly suited to investigate excited-state processes because it directly interrogates the evolving electronic structure along a reaction coordinate.[1] Electron spectroscopy offers spectroscopic data against an absolute energy scale (the energy of the electron in vacuum) and can therefore remove ambiguities in the assignment of molecular states as compared with purely optical detection methods. TRPES was used with great success to observe intramolecular processes in isolated molecules. (See ref 2 and references therein.) Being feasible only in vacuo, this technique seems unsuited to investigate biological systems where intermolecular interactions may play a dominant role. We try to bridge this gap with the investigation of isolated molecular clusters, which reproduce specific structural elements and photochemical reaction coordinates relevant to biological systems. Here we present the direct spectroscopic characterization of an intermolecular hydrogen transfer reaction by time-resolved photoelectron and mass spectroscopy.

No methods exist to produce size-selected molecular clusters, and hence photoelectron studies are more common for anionic clusters where a cluster separation by mass/charge ratio is possible before photoionization. (See ref 3 for examples.) To address neutral clusters, we employ electron−ion coincidence spectroscopy,[4] that is, ionize a molecular cluster of unknown size and detect the mass of the cluster ion and the energy of the emitted photoelectron for this single ionization event. This allows the investigation of neutral clusters but only for very low ionization rates. To combine such a technique with the low duty cycle of pulsed femtosecond lasers in time-resolved pump−probe experiments sounds counterintuitive but combines several powerful spectroscopic tools and was used to investigate a number of small systems, such as ammonia clusters,[4] NO dimer,[5] benzene dimer,[6] and adenine−thymine base pairs.[7]

Theory predicted a particularly interesting excited-state reaction pathway in 2-aminopyridine dimers, where conical intersections couple a locally excited (LE) and a charge transfer (CT) state along a proton transfer coordinate. The coupled electron and proton transfer reaction results in a net hydrogen transfer and may offer a conduit for ultrafast electronic relaxation (via back H transfer) into the electronic ground state.[8] The resulting short excited-state lifetime could preclude photochemical reactions and therefore serve to increase the photostability of this and other hydrogen-bonded systems. The same relaxation mechanism was proposed for the Watson−Crick structures of DNA base pairs[9,10] and may have played an evolutionary role in protecting these essential biological building blocks from photochemical damage.[11]

We identified an accelerated excited-state relaxation in 2-aminopyridine dimers by time-resolved mass spectroscopy.[12] Large isotope effects for the *N*,*N*-dideuterated species confirmed the important role of the N−H mode in the relaxation mechanism[13] and identified a surprising increase in the excited-state lifetime with excitation energy. Here we present a direct spectroscopic characterization of the transient states in aminopyridine monomer and dimer by coincidence photoelectron spectroscopy. The detailed spectroscopy, together with ab initio calculations, confirmed the role of the intermolecular H transfer and allowed the assignment of two novel ultrafast reaction channels for the monomer and dimer at higher excitation energies.

II. Materials and Methods

A. Mass and Electron Spectroscopy. 2-Aminopyridine (AP) powder (Sigma Aldrich, 99% purity) was evaporated at 60−80 °C, entrained in helium as carrier gas, and expanded into a vacuum spectrometer. Supersonic expansion through a pulsed valve (General valve series 9) running at ≤200 Hz led to the formation of $(AP)_n$ clusters. The width of the cluster distribution was controlled by the helium pressure (1 to 1.5 bar), the pulsed-valve opening time, and the delay between pulsed molecular beam and pump laser pulse.

Two focused copropagating laser beams with pulse durations of ∼80 fs crossed the skimmed molecular beam. The molecules were excited (pumped) at λ_{ex} = 250, 274, 292, and 296 nm and

* Corresponding author. E-mail: schultz@mbi-berlin.de.

10.1021/jp903460b CCC: $40.75
Published on Web 07/01/2009

subsequently probed by one- or multiphoton ionization with λ_{pr} = 400 or 800 nm. The time delay between pump and probe pulses was adjusted with a mechanical delay line to probe the temporal evolution of the excited state. Ions and electrons were collected by time-of-flight spectrometers: the kinetic energy of emitted electrons was determined in a magnetic bottle photoelectron spectrometer, and the cluster ion mass was characterized in a Wiley−McLaren mass spectrometer. Electrons and ions were detected by multichannel-plate detectors with respective quantum efficiencies of 40 and 35%.

To obtain electron spectra for mass-selected cluster species, we must revert to coincidence spectroscopy and detect coinciding electrons and ions that can be assigned to single ionization events. This is possible for low ionization rates of ~10%, where the probability of false coincidences becomes very small (i.e., the detection of one electron and one ion from two separate ionization events can be neglected).[14] One-color, multiphoton pump-only and probe-only spectra were measured independently and subtracted. We want to stress that this experiment is very time-consuming because of the limited repetition rate of the pulsed valve, the low ionization rates, and the limited quantum yield for electron/ion detection. We collect coincidences at a rate of only a few hertz, and the signal in one selected cluster mass channel is only a small fraction of the total coincidence signal. The signal-to-noise ratio of the resulting electron spectra is therefore limited, and we measured electron spectra at pump−probe delays of only zero (temporal overlap of pump and probe beams) and 20 ps. For easier viewing, the oversampled spectra were smoothed in origin. Signals without smoothing and before subtraction of the pump-only and probe-only spectra can be found in the Figures 1 and 3 of the Supporting Information. We calibrated electron energies by comparing measured ionization potentials (IPs) for nitric oxide and toluene with literature values.

To analyze excited-state dynamics in detail, we measured time-resolved mass spectra with higher ionization rates, as described elsewhere.[13] Small amounts of indole or toluene were added for calibration purposes and to determine the zero delay time between excitation and ionization pulses.

B. Computational Details. Ab initio calculations were carried out with the TURBOMOLE[15] and MOLPRO[16] software packages using the aug-cc-pVDZ basis set and C_1 symmetry. We determined the energies of the neutral ground and excited electronic states with the help of the second-order approximate resolution-of-identity coupled cluster method (RI-CC2).[17] This method failed for the cation because of low-lying excited states. Therefore, IPs were determined with the complete active space second-order perturbation theory (CASPT2).[18] We included three orbitals in the active space of our CASPT2 calculations: the highest occupied π and n and the lowest unoccupied π^* orbitals. Geometry optimizations were conducted at the RI-MP2 level (second-order resolution-of-identity Moller−Plesset theory[19]) for the determination of IPs and at the RI-CC2 level for the calculation of electronic excitation energies.

III. Results

A. Time-Resolved Mass Spectroscopy. The excited-state dynamics for AP monomer and clusters excited at 296 (4.19 eV), 293 (4.23 eV), 274 (4.53 eV), and 250 nm (4.96 eV) and probed with 800 nm have been previously discussed.[12,13] For excitation of the AP monomer close to the $^1\pi\pi^*$ state origin at 299 nm (4.15 eV) and down to a wavelength of 274 nm (Figure 1A), our spectra reproduced the nonradiative lifetime τ_1^{mon} = 1.5 ns estimated from the line width in rotational spectra.[20] A

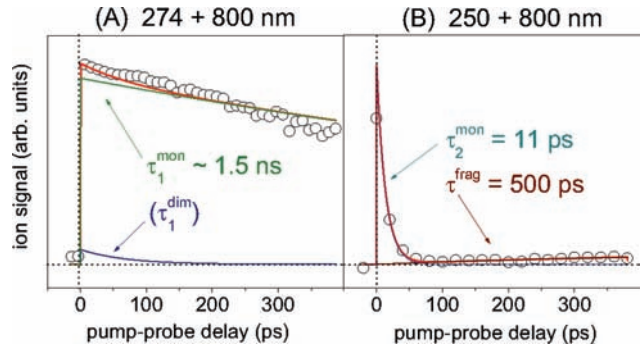

Figure 1. Aminopyridine monomer ion signal as a function of the delay time between (A) 274 and (B) 250 nm excitation pulses and 800 nm ionization pulses. The experimental data (○) were fitted by a sum of exponentially rising and decaying traces (—). Lifetimes τ_1^{mon} and τ_2^{mon} were assigned to transient excited states of aminopyridine monomer, whereas τ_1^{dim} and τ^{frag} are due to fragmenting clusters. (See text.)

small transient signal with lifetime τ_1^{dim} = 75 ps was assigned to excited-state dynamics in the dimer, a fraction of which fragmented after ionization. The fragment signals were much more prominent in molecular beams with broader cluster distribution, as can be seen in previously published data.[12,13]

Upon excitation at 250 nm, we observed much faster excited-state relaxation and a lifetime of τ_2^{mon} = 11 ps (Figure 1B). The origin of this fast excited-state decay will be discussed in context of the ab initio calculations below. After 250 nm excitation, bigger clusters had enough energy to fragment in the neutral excited state, and the monomeric fragmentation product was probed by ionization with the delayed probe pulse. This fragmentation channel lead to a small rising signal with $\tau^{frag} \approx$ 500 ps. A corresponding signal was not observed for excitation wavelengths ≥274 nm, presumably because the vibrational excess energy was not sufficient for cluster dissociation on the sub-nanosecond time scale. Depending on the width of the cluster distribution and the relative pump and probe laser intensities, we also observed fragmentation of the ionic clusters, as described for 274 nm excitation. Changing the wavelength of the probe pulses did not affect the observed dynamics in the monomer.[30]

For an excitation wavelength of 274 nm or longer, the excited-state relaxation in the dimer was orders of magnitude faster than that in the monomer. We observed monoexponential decays with lifetimes of τ_1^{dim} = 50 to 90 ps (Figure 2A, see also ref 13). A small transient signal with a nanosecond lifetime (τ^{frac}) could be assigned to the fragmentation of larger clusters in the ionic state. The amplitude of this signal is proportional to the amplitude of signals in the AP trimer and bigger mass channels and vanished for very narrow cluster distributions. For excitation at 250 nm, we observed τ_1^{dim} as described above and an additional ultrafast component with lifetime $\tau_2^{dim} \leq$ 50 fs (Figure 2B, inset). The amplitude of this ultrafast component was drastically enhanced relative to the τ_1^{dim} signal when the ionization wavelength was changed from 800 to 400 nm (Figure 3B). But a corresponding signal was not observed for excitation with wavelengths ≥274 nm, irrespective of the ionization process (Figure 3A).

B. Coincidence Photoelectron Spectroscopy. We measured pump−probe photoelectron−ion coincidence spectra to investigate the electronic character of the monomer and dimer states. To characterize the femtosecond and picosecond transients observed in the time-resolved mass spectra, we measured photoelectron spectra at pump−probe delays of 0 and 20 ps.

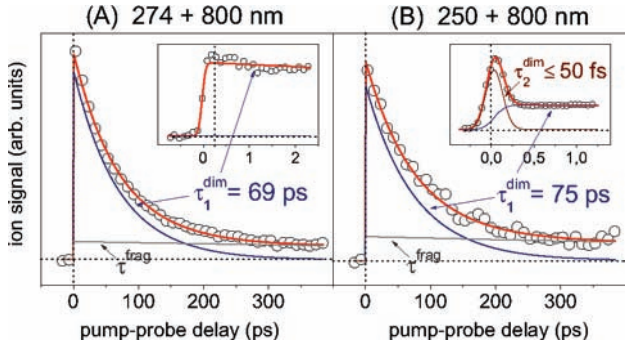

Figure 2. Time-resolved ion signals for aminopyridine dimer with (A) 274 or (B) 250 nm excitation and 800 nm ionization. Exponential fits (—) to the experimental data (○) revealed picosecond decays with τ_1^{dim} and a long-lived component with $\tau^{frag} \approx 1.5$ ns due to fragmentation of larger clusters into the dimer mass channel. An additional short-lived component with τ_2^{dim} was observed for 250 nm excitation but not for excitation with 274 nm or above. (see insets).

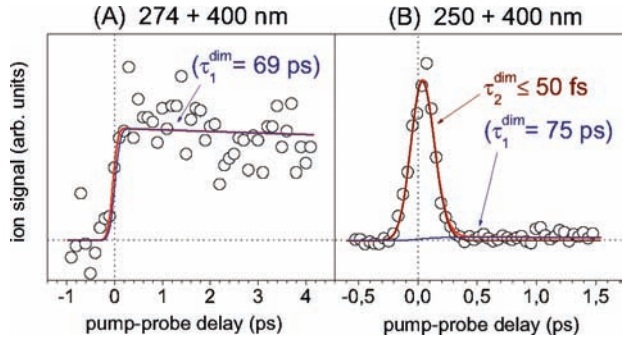

Figure 3. Time-resolved ion signals for aminopyridine dimer excited with (A) 274 or (B) 250 nm and ionized with 400 nm. Signals (○) and fits (—) for data with 274 nm excitation reproduced our observations with 800 nm ionization (cf. Figure 2A, inset), and the short-lived trace with τ_2^{dim} is absent. For 250 nm excitation, the changed ionization process strongly enhanced the signal with lifetime τ_2^{dim} relative to that with τ_1^{dim} (cf. Figure 2B, inset) and the respective monomer signal (not shown).

Figures 4 and 5 show the photoelectron spectra for 274 and 250 nm excitation and 400 nm ionization. In the spectral region of low electron kinetic energies (EKEs), the subtraction of large one-color signals degraded the signal-to-noise ratio considerably. (Unsubtracted photoelectron spectra for the monomer and coincident mass spectra are shown in the Supporting Information.)

The monomer spectra for 274 nm excitation (0.37 eV above the $^1\pi\pi^*$ state origin) are broad and show a slightly anharmonic vibrational progression with a level spacing of approximately 300 meV (Figure 4A). The spectra for pump−probe delays of 0 and 20 ps are nearly identical. The law of energy conservation allows us to calculate electron binding energies (BEs) corresponding to the measured EKEs for the observed 1 × (274 nm) + 2 × (400 nm) ionization process.[31] Barring unfavorable Franck−Condon factors, the lowest observed BE (BE_{thresh}, corresponding to the highest observed EKE) should correspond to the adiabatic IP. From our spectrum, we estimate a threshold value of $BE_{thresh} = 8.45$ eV, which is well above the literature value of $IP_{ad} = 8.11$ eV,[21−23] and hence adiabatic ionization is not observed. The energy difference between the adiabatic IP and the first band observed here is ~0.35 eV and corresponds almost exactly to the excess energy in the photoexcited neutral. Our vertical IP for excited-state ionization is much higher than the literature value of 8.34 eV for ground-state ionization.[24]

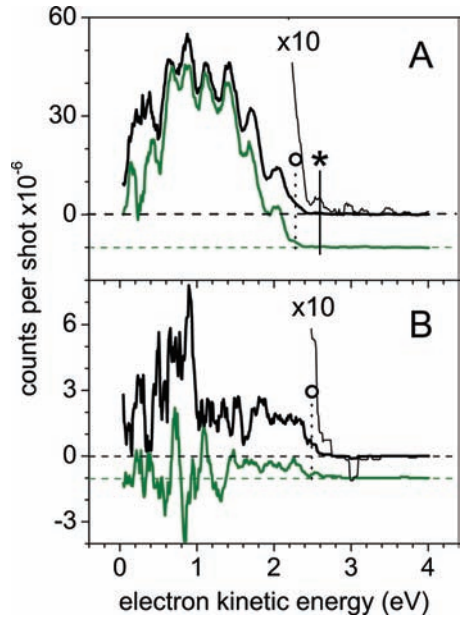

Figure 4. Electron spectra of (A) AP monomer and (B) AP dimer with 0 and 20 ps delay between 274 nm excitation and 2× (400 nm) ionization. Spectra at pump−probe delays of 20 ps carry a negative offset for easier viewing. Symbols mark the position of the adiabatic ionization potential (*) reported in the literature[21−23] and the threshold of the first strong band in our spectra (○, used to calculate BE_{thresh}, as described in the text).

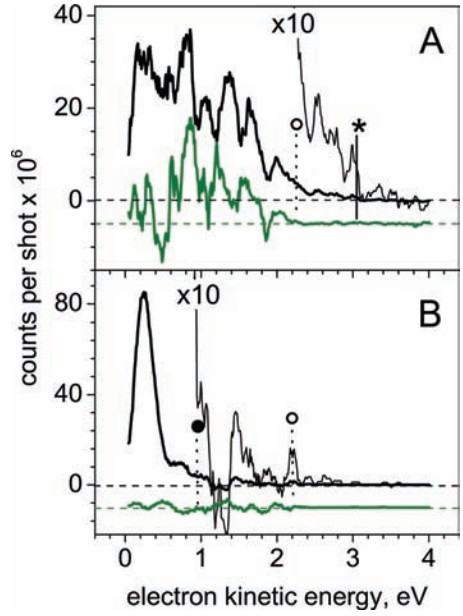

Figure 5. Electron spectra with 250 nm excitation, as in Figure 4. (A) In the monomer, the edge of a weak photoelectron band coincides with the adiabatic ionization potential (*), but the threshold of the first prominent band (○) is observed at 0.80 eV lower electron kinetic energy. (B) In the dimer signal, the corresponding [1 + 2′] photon signals with a threshold of 2.25 eV (○) are weak, and the spectrum is dominated by a lower-order [1 + 1′] photon ionization process with electron kinetic energies ≤0.95 eV (●).

The dimer spectra (Figure 4B) are broad and show a threshold binding energy red-shifted by about 0.25 eV relative to that of the monomer. The amplitude of the electron signal at a pump−probe delay of $\Delta t = 20$ ps is considerably lower than that at $\Delta t = 0$ ps, which is in agreement with the time dependence observed in the ion signals (cf. Figures 1 and 2). In the spectrum for $\Delta t = 0$, the noisy band at EKE < 1 eV may

TABLE 1: Comparison of Calculated (E_{calcd}) and Experimental (E_{exptl}) Energies (in electronvolts) for the Aminopyridine Monomer and Dimer[a]

state	E_{calcd}	E_{exptl}
monomer		
$^1\pi\pi^*$ origin	4.253	4.150(1)
crossing $^1\pi\pi^*-^1n\pi^*$	4.75	4.53−4.96(2)
IP_{ad} ($^2\pi$)	8.084	8.109(3), 8.1(2)
IP_{vert} ($^2\pi$)	8.447	8.34(4)
dimer		
$^1\pi\pi^*$ origin	3.999	3.944(5)
IP_{ad} ($^2\pi$)	6.943	7.1(2)

[a] Experimental values are taken from (1)Borst et al.,[20] (2)our results (see text), (3)threshold ionization experiments,[22,23] (4)Kobayashi et al.,[24] and (5)Wu et al.[28]

be due to errors in the subtraction of large one-color signals and will not be further discussed.

Pump−probe photoelectron spectra for AP monomer upon 250 nm excitation (0.81 eV above the $^1\pi\pi^*$ origin) are again broad (Figure 5A) and show a vibrational progression comparable to that observed with 274 nm excitation. The spectrum at zero delay is dominated by prominent bands ≥0.80 eV above the adiabatic IP, but the latter is observed as the threshold of a small band in our spectra. (See 10× magnified signal in Figure 5A.) The amplitude of the monomer signal at a pump−probe delay of 20 ps is very small, reflecting the fast signal decay observed in the time-resolved mass spectra (cf. Figure 1B).

The photoelectron spectrum measured for the dimer with 250 nm excitation (Figure 5B) is drastically different from both the monomer spectrum and that measured for the dimer with 274 nm excitation. A strong band with EKE < 1 eV is assigned to a lower-order 1 × (250 nm) + 1 × (400 nm) ionization process. This strong band is not observed at a delay of 20 ps. The comparison of amplitudes at delays $\Delta t = 0$ and 20 ps with those in the corresponding mass spectra (cf. Figure 3B) directly imposes an assignment of this band to the short-lived transient with $\tau_2^{dim} \leq 50$ fs. The $1 + 2'$ photon signal is also present but is almost two orders of magnitude weaker than that of the lower-order process. From the observed $1 + 1'$ ionization threshold (EKE ≤ 0.95 eV), we estimate an adiabatic ionization potential $IP_{ad}^{dim} = 7.1$ eV for the short-lived transient. The origin of this transient species with low IP will be discussed below, taking the results of ab initio calculations into account.

C. Ab Initio Calculations. Table 1 compares excited- and ionic-state energies to experimental values where applicable. In the neutral electronic ground state of the monomer, the aminopyridine ring is nearly planar, and the amino group is slightly tilted with respect to it. This agrees with published microwave spectra from Kydd and Mills, who estimated a tilt angle of 31.6°,[25] and later spectra are also consistent with a nonplanar ground state.[26] We calculated a vertical IP of 8.447 eV for the equilibrium geometry of the neutral ground state, close to the literature value of 8.34 eV.[24] The geometry of the cationic ground state is perfectly planar, and the calculated adiabatic IP of 8.084 eV is in very good agreement with the corresponding experimental value of 8.109 eV obtained by mass-analyzed threshold ionization.[22,23]

Our calculated vertical transition energy from the electronic ground to the lowest excited $^1\pi\pi^*$ state was 4.578 eV. For the adiabatic transition energy, we found 4.253 eV, which is in good agreement with the measured value of 4.150 eV.[20,27] The corresponding equilibrium geometry is planar, and the calculated vertical IP for this geometry is 8.280 eV, lower than the vertical IP from the ground state. The calculated vertical excitation energy of the lowest $^1n\pi^*$ state is 5.234 eV, that is, above the excitation energies in our experiments. A conical intersection of the $^1\pi\pi^*$ and $^1n\pi^*$ states is found at almost planar geometry at an energy of 4.75 eV and is therefore accessible with 250 nm excitation. The energy of the $^1n\pi^*$ state decreases further with increasing nonplanarity.

The calculated equilibrium geometry of the hydrogen-bound dimer in the ground electronic state is almost planar, apart from a slight tilt of the amino groups. The excitation energy of the LE $^1\pi\pi^*$ states is ∼0.2 eV lower than that in the monomer; we found a vertical transition energy of 4.364 eV. No bright higher excited states accessible by the experimental excitation energies were found. The calculated $^1\pi\pi^*$ adiabatic excitation energy of 3.999 eV coincides nicely with the measured 0−0 transition frequency of 3.944 eV.[28] In addition to the LE states of the monomers, Sobolewski et al. predicted a low-lying CT $^1\pi\pi^*$ state in the dimer.[8] In the CT state, one electron from the π orbital of one molecule is promoted to the π^* orbital of the other molecule. The equilibrium geometries of the CT state predicted by Sobolewski et al. and of a second CT* state identified in our calculations show a characteristic proton transfer from the amine group of one moiety to the ring nitrogen of the other. The adiabatic energy of the lowest CT $^1\pi\pi^*$ state was calculated to be 3.040 eV, and the corresponding energy of the next higher CT* $^1\pi\pi^*$ state was 4.024 eV.

CASPT2 calculations for aminopyridine dimer were carried out including six orbitals in the active space: the two highest occupied π and n orbitals and the two lowest unoccupied π^* orbitals. We calculated a vertical IP of 7.957 eV for the ground-state equilibrium geometry and an IP of 7.805 eV for the LE $^1\pi\pi^*$ state equilibrium geometry. The global minimum in the cationic dimer has a proton transfer geometry similar to that of the CT and CT* states.[32] We determined the corresponding adiabatic IP to be 6.943 eV. A local minimum with an IP of 7.326 eV exists in the non-proton transfer geometry.

Although the conical intersection between the LE and CT electronic states of $(2\text{-AP})_2$ has been theoretically investigated before,[8] a more detailed discussion is in order because the corresponding minimum energy profiles were calculated only in dependence of the N−H reaction coordinate, and all remaining coordinates were geometry optimized while preserving a planar structure. The resulting reaction coordinate can be misleading if large geometry changes occur in other coordinates along the reaction path. A crucial coordinate in this respect is the intermolecular vibration, which has a large reduced mass and a small zero-point vibrational amplitude. This slow intermolecular mode can be assumed to remain frozen on the time scale of ultrafast processes. Therefore, it may be beneficial to illustrate the energy profile of the hydrogen transfer in dependence of two coordinates: the N−H reaction coordinate and the adjacent intermolecular N···N distance of the two constituents. We investigated the potential energy surfaces for the lowest $^1\pi\pi^*$ LE and CT states along the r(N−H) proton transfer coordinate for three fixed intermolecular distances r(N···N) = 2.6, 2.8, and 3.0 Å with optimized geometry for all remaining coordinates. The largest N···N distance of 3.0 Å is close to the equilibrium distance in the electronic ground state and therefore the geometry for vertical excitation, whereas the intermediate value of 2.8 Å is close to the equilibrium distance in the $^1\pi\pi^*$ LE state. We find that the electron/proton transfer barrier is sensitive to the N···N distance and increases significantly with the intermolecular separation.

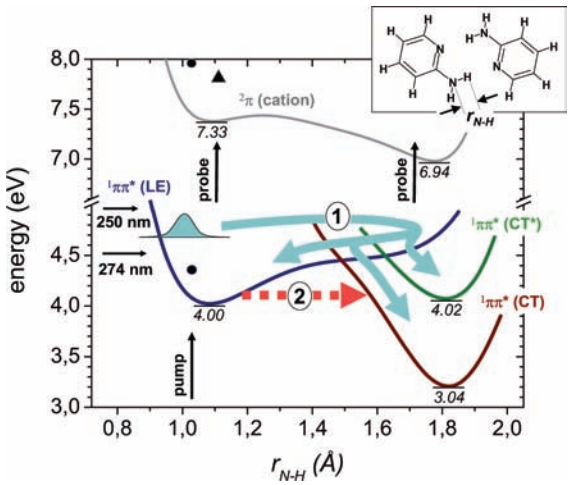

Figure 6. Calculated potential energy surfaces of aminopyridine dimer along the proton transfer coordinate for a fixed intermolecular distance $r(\mathrm{N\cdots N}) = 2.8$ Å. Solid symbols mark the calculated vertical ionization potential from the excited state (▲, 7.81 eV) and the vertical excitation and ionization energies from the ground state (●, 4.36 and 7.96 eV). Expected/observed excited-state population dynamics are illustrated by blue arrows: After excitation from the ground state with 250 nm (pump), vibrational dynamics ① allow the observation of a transient signal from the proton-transfer geometry. The latter is efficiently probed by one-photon ionization and may stem from the $\pi\pi^*$ (LE) and $\pi\pi^*$ (CT*) states. Residual population in the LE state decays on a 70−90 ps time scale ② via the $\pi\pi^*$ (CT) state, as does the population after excitation with 274 nm.

Figure 6 shows the calculated potential energy surfaces of the low-lying $^1\pi\pi^*$ LE, CT, and CT* states and the lowest cationic $^2\pi$ state as a function of the N−H bond length for the N···N distance of 2.8 Å. Excitation with 274 and 250 nm deposits considerable vibrational energy (0.58 and 0.98 eV, respectively) into the excited state. For predominantly vertical excitation from the ground state with $r(\mathrm{N\cdots N}) \approx 3.0$ Å and $r(\mathrm{N-H}) \approx 1.03$ Å, this excess energy should only result in modest vibrational excitation along the N−H reaction coordinate and the intermolecular N···N stretch mode. A considerable barrier has to be overcome for a transition from the LE state to the CT states, but we stress again that this barrier is modulated by the intermolecular stretch vibration. There is a large difference between the equilibrium geometry of the LE $^1\pi\pi^*$ state and that of the cationic $^2\pi$ state, the latter having a proton transfer geometry. The expected cross section for LE $^1\pi\pi^*$ ionization into low vibrational levels of the cationic ground state should therefore be small. Ionization into the $^2\pi$ adiabatic ground state should be observed only after considerable excitation of the N−H stretch vibration or after an electronic transition into the CT* $^1\pi\pi^*$ state.

IV. Discussion

A. Aminopyridine Monomer. Comparing the time-dependent ion signals of the 2-aminopyridine monomer for the excitation wavelength of ≥274 and 250 nm (cf. Figure 1), we find an excited-state lifetime of $\tau_1^{\mathrm{mon}} = 1.5$ ns for the former case and $\tau_2^{\mathrm{mon}} = 11$ ps for the latter case. Our calculation has shown no indication of an additional higher-lying electronic state accessible by vertical excitation from the ground state, and hence we probe the same $^1\pi\pi^*$ state in all experiments. The accelerated population decay at higher excitation energy may be explained by relaxation via the $^1n\pi^*$ state to the electronic ground state: the calculated conical intersection between the $^1\pi\pi^*$ and $^1n\pi^*$ state is accessible at energies >4.75 eV (i.e., with 250 nm excitation). The excitation energy at 274 nm (4.53 eV) is below the calculated conical intersection, and relaxation via the $^1n\pi^*$ state is not expected.

The photoelectron spectra for the monomer (Figures 4A and 5A) show ionization into the $^2\pi$ electronic ground state of the ion. Our observed threshold IPs after 274 and 250 nm excitation were 0.35 and 0.80 eV above the literature value for the adiabatic IP,[21–23] and the latter was only observed as the edge of a small band. The differences between threshold and adiabatic IPs correspond almost exactly to the vibrational excess energy in the excited state and may indicate a similar geometric and vibrational structure in the excited and ionic states (and a largely diagonal Franck−Condon matrix). A strong vibrational progression with a level spacing of ∼2400 cm^{-1} (0.300 eV) and the strongly shifted vertical IP, however, indicate that this is not true for all vibrational degrees of freedom. Preliminary calculations suggest that the observed progression may be due to amine−imine tautomerization in the $^1\pi\pi^*$ state. The $^1\pi\pi^*$-state energy is considerably lower for 2(1*H*)-pyridinimine than for 2-aminopyridine. Remarkably, a theoretical paper investigating this and other nonradiative decay channels in detail[29] was published very recently during the extended refereeing stages of our manuscript. For the ionization of the pyridinimine into the aminopyridine cation, we expect a broad Franck−Condon progression in the tautomerization coordinate.

At first glance, the proposition of an excited-state tautomerization is in contradiction with the largely diagonal Franck−Condon matrix discussed above. But motion along the N−H tautomerization coordinate may lead to $\nu_n \rightarrow \nu_{n+x}$ transitions, with x being dominantly positive (transitions to higher vibrational states in the ion), as might be expected if the inner turning point of the N−H motion is unchanged and the outer turning point is strongly changed. The other 33 vibrational degrees of freedom still dominate the observed threshold IP (simple state−density arguments apply) and lead to the quasi-linear shift of the ionization threshold with the excitation energy. This model explains the observed photoelectron spectra and agrees qualitatively with expectations from the ab initio calculations. This description is only qualitative, and indeed the photoelectron spectra show weak bands between the adiabatic and the observed "threshold" IPs. A detailed Franck−Condon simulation would be desirable, and we hope that the experimental results will attract the curiosity of qualified theoretical groups.

B. Aminopyridine Dimer. In the dimer, the relevant hydrogen and nitrogen atoms form hydrogen bonds to the neighboring aminopyridine molecule. A tautomerization in the dimer would require the breaking of both hydrogen bonds and is therefore energetically unfavorable. Instead, we must consider the intermolecular hydrogen transfer coordinate and CT states, as shown in Figure 6.

The excited-state relaxation of AP dimer excited at ≥274 nm occurs with a lifetime of $\tau_1^{\mathrm{dim}} \approx 70$ ps via the CT $^1\pi\pi^*$ state (cf. Figure 2). The relatively long lifetime of the lowest LE $^1\pi\pi^*$ state is explained by a considerable energetic barrier for the internal conversion process (ref 13 and Figure 6). The transient population in the CT $^1\pi\pi^*$ state decays quickly to the electronic ground state and is therefore not observed in time-resolved mass or electron spectra. The photoelectron spectrum measured with 274 nm excitation confirms this model: only population from the LE $^1\pi\pi^*$ state is observed. The observed threshold IP of ∼8.2 eV for the 1 × (274 nm) + 2 × (400 nm) ionization process agrees reasonably well with the calculated $^1\pi\pi^*$ vertical value of 7.8 eV, in particular, if we account for the vibrational excess energy in the excited state

which may be preserved upon ionization. The situation therefore resembles that in the monomer.

With 250 nm excitation, we observed an additional ultrafast transient with a lifetime $\tau_2^{dim} \leq 50$ fs (Figures 2B and 3B). The corresponding photoelectron spectra showed a band at low EKE and were markedly different from those of the monomer or that of the dimer with 274 nm excitation. In the following, we briefly discuss the assignment of this signal. As seen from the ordinate in Figure 4, the integrated electron signal of the monomer excited with 274 nm is more than 20 times larger than the corresponding signal of the dimer. If we assume comparable ionization efficiencies for both species, then this ratio reflects the concentration of both species in the molecular beam. The observed ratio agrees with our expectations for the chosen molecular beam conditions, and the observed cluster spectrum is independent of the ionization process. (See one- and two-color mass spectra in the Supporting Information.) With 250 nm excitation, however, the signal amplitudes for monomer and dimer are almost equal because of the large amplitude of the ultrafast transient. The large amplitude signal in the dimer is not due to an increased dimer concentration in the molecular beam, as was ascertained by comparing the one-color, 400 nm signals for both experiments. (See the Supporting Information.) The large signal must therefore be assigned to an increased ionization cross section for the dimer after 250 nm excitation.

The calculated potential energy surfaces (Figure 6) offer a satisfactory explanation for our observations: if enough vibrational energy is deposited in LE $^1\pi\pi^*$ state, then the vibrational wave function may extend into the region of large N−H distances along the proton-transfer coordinate. Near the outer turning point of this coordinate, we may expect a considerable overlap with the vibrational ground state of the cation. The corresponding low adiabatic IP in the dimer allows a lower-order $1 \times (250\text{ nm}) + 1 \times (400\text{ nm})$ ionization process with correspondingly larger cross-section as compared with the $2 \times (400\text{ nm})$ ionization process in the monomer or at the longer probe wavelength of 800 nm. Indeed, the observed threshold IP of 7.1 eV for the dimer is close to the calculated value of 6.95 eV for adiabatic ionization in the proton transfer geometry. Please note that we would not expect such a low IP for the ionization of any state in the non-proton transfer geometry. The comparison of Figures 2B (probe wavelength of 800 nm) and 3B (probe wavelength of 400 nm) shows that the order of the ionization process has a drastic effect on the relative amplitudes of the signals from the proton-transfer geometry and the LE geometry: upon ionization with 800 nm, the enhancement in ionization cross section for the proton-transfer geometry is partially lost, and the short-lived τ_2^{dim} transient is less dominant.

Considering the calculated potential energy surfaces in Figure 6, we expect small Franck−Condon factors for excitation of the LE $^1\pi\pi^*$ N−H stretch vibrational states that extend into the proton-transfer geometry, but this excitation cross section may be enhanced if electrical anharmonicity and Herzberg−Teller coupling with the next excited LE $^1\pi\pi^*$ state (located slightly above 5 eV according to our ab initio calculations) is taken into account. Also, it is sufficient if only a small fraction of the optically excited dimers show excitation of the N−H stretch vibration: the efficiency for ionization by one probe photon may be several orders of magnitude larger than that for ionization by two probe photons, thus enhancing the corresponding signals.

Next, we must address the ultrafast decay ($\tau_2^{dim} \leq 50$ fs) of the adiabatic ionization channel in the proton transfer geometry. One conceivable explanation is rapid intramolecular energy redistribution within the 73 vibrational degrees of freedom in the dimer, which effectively removes the population from the proton transfer region of the LE $^1\pi\pi^*$ surface. But the large amplitude N−H stretch vibration in the LE $^1\pi\pi^*$ state also crosses two conical intersections with the CT and CT* states. With typical NH stretch frequencies of 3400 cm^{-1} (corresponding to a period of less than 10 fs, albeit the frequency in the excited-state may be lower), we may expect that the conical intersections are reached within less than 50 fs. Because these conical intersections lie in the classically allowed region, the corresponding nonadiabatic coupling may reduce the lifetime of a subset of vibrationally excited levels in the LE $^1\pi\pi^*$ state to less than 50 fs. The equilibrium geometry of both CT states is similar to that of the cation. If we assume that the vibrational excess energy in the CT or CT* states is conserved in the ionization step (corresponding to a diagonal Franck−Condon matrix as described for the monomer above), then we would expect to observe a threshold IP at 0.9 and 1.9 eV above the adiabatic value. Ionization of the CT* state may therefore be responsible for part of the large band observed at electron kinetic energies ≤0.3 eV, but ionization of the lower CT state requires two probe photons, and corresponding signals are expected to be weak. The population in the CT* state may rapidly decay by nonadiabatic coupling to the CT state and by back-electron transfer into the electronic ground state.

Therefore, we understand why the photoelectron signal with low ionization threshold of 7.1 eV vanishes rapidly, but it remains mysterious why the remaining fraction of the population in the LE $^1\pi\pi^*$ state after 250 nm excitation has a larger lifetime (75 ps) than the LE $^1\pi\pi^*$ population after 293 or 274 nm excitation (50 or 69 ps, respectively[13]). We can only offer a tentative explanation based on the calculated potential energy surfaces, which predict a considerable barrier for internal conversion from the LE $^1\pi\pi^*$ to the CT $^1\pi\pi^*$ state. This barrier is increasing with the intermolecular distance $r(N\cdots N) = 2.6$, 2.8, and 3.0 Å. We also expect that other intermolecular modes, which were not investigated explicitly, affect the barrier and the tunneling probability for the hydrogen atom. By increasing the vibrational excess energy in the excited state, we also excite the low frequency intermolecular modes and thus directly affect the reaction coordinate and reaction rate. The observed rates indicate a "narrow tunnel" for LE to CT internal conversion; that is, only a small region on the potential energy surface allows fast proton tunneling, and this region is preferentially accessed by a more localized wave function at low excess energies. It is an open question whether the anharmonicity of the intermolecular modes also plays a role: excitation of the intermolecular stretch might increase the intermolecular distance and therefore the average barrier for internal conversion. In the extreme case, the anharmonic stretch may lead to the breaking of one or both hydrogen bonds, and we point out that we indeed observed cluster fragmentation in the neutral excited state after 250 nm excitation (cf. transient with τ^{frag} in Figure 1B).

In conclusion, the following excited-state processes can be derived from our spectroscopic, dynamic, and theoretical investigation of the 2-aminopyridine dimer: Excitation of the LE $^1\pi\pi^*$ state with a femtosecond pump pulse at 250 nm is followed by electronic relaxation via two pathways. (See Figure 6.) A fraction of the excited-state population with sufficient energy in the N−H stretch vibration crosses into the proton transfer geometry ①, where it can be ionized into the cationic ground state by absorption of only one 400 nm probe photon. Internal conversion into the CT or CT* state (corresponding to electron transfer from the proton donor to the proton

acceptor and thus a net hydrogen transfer reaction) may offer a pathway for ultrafast electronic relaxation with $\tau_2^{dim} \leq 50$ fs. Some population remains trapped in the LE $^1\pi\pi^*$ state which is detected with lower efficiency by two photon ionization. This population decays by nonadiabatic tunneling through a barrier ② with $\tau_1^{dim} \approx 75$ ps to the CT $^1\pi\pi^*$ state. The latter is crossing the ground state at larger N−H and N···N distances[8,12] and should be very short-lived. Path ② is the only one open for longer pump wavelengths $\lambda_{pu} \geq 274$ nm. An accelerated excited-state relaxation of the monomer $^1\pi\pi^*$ state at high excitation energies was assigned to an internal conversion to the $^1n\pi^*$ state via conical intersection. No evidence of a comparable process was found in the dimer.

The thorough study presented here shows how the correlated measurement of spectroscopic and dynamic properties allows us to disentangle complex excited-state processes. The characterization of a molecular dimer, however, is already pushing the employed techniques to their limit. The diagnosis of cluster fragmentation, in particular, makes the characterization of larger cluster species difficult.

For the monomer and dimer, we found an excellent agreement between calculated excited- and ionic-state energies and experimental data presented here and in the literature. (See Table 1.) We therefore demonstrated that the detailed characterization of an intermolecular reaction in a molecular dimer is feasible with state of the art experimental and theoretical methods.

Acknowledgment. We thank Dr. F. Noack for his support by providing the laser system in the femtosecond application laboratory of the Max-Born-Institut Berlin. Financial support by the Deutsche Forschungsgemeinschaft through SFB-450 is gratefully acknowledged.

Supporting Information Available: Coincidence photoelectron spectra of 2-aminopyridine monomer and coincidence mass spectra of 2-aminopyridine clusters. This material is available free of charge via the Internet at http://pubs.acs.org.

References and Notes

(1) Blanchet, V.; Zgierski, M. Z.; Seideman, T.; Stolow, A. *Nature* **1999**, *401*, 52–54.
(2) Stolow, A.; Bragg, A. E.; Neumark, D. M. *Chem. Rev.* **2004**, *104*, 1719–1757.
(3) Neumark, D. M. *J. Chem. Phys.* **2006**, *125*, 132303.
(4) Stert, V.; Radloff, W.; Schulz, C. P.; Hertel, I. V. *Eur. Phys. J. D* **1999**, *5*, 97–106.
(5) Gessner, O.; Lee, A. M. D.; Shaffer, J. P.; Reisler, H.; Levchenko, S. V.; Krylov, A. I.; Underwood, J. G.; Shi, H.; East, A. L. L.; Wardlaw, D. M.; Chrysostom, E. T.; Hayden, C. C.; Stolow, A. *Science* **2006**, *311*, 219–222.
(6) Radloff, W.; Stert, V.; Freudenberg, T.; Hertel, I. V.; Jouvet, C.; Dedonder-Lardeux, C.; Solgadi, D. *Chem. Phys. Lett.* **1997**, *281*, 20–26.
(7) Gador, N.; Samoylova, E.; Smith, V. R.; Stolow, A.; Rayner, D. M.; Radloff, W.; Hertel, I. V.; Schultz, T. *J. Phys. Chem. A* **2007**, *111*, 11743–11749.
(8) Sobolewski, A. L.; Domcke, W. *Chem. Phys.* **2003**, *294*, 73–83.
(9) Sobolewski, A. L.; Domcke, W.; Hättig, C. *Proc. Natl. Acad. Sci. U.S.A.* **2005**, *102*, 17903–17906.
(10) Perun, S.; Sobolewski, A. L.; Domcke, W. *J. Phys. Chem. A* **2006**, *110*, 9031–9038.
(11) Abo-Riziq, A.; Grace, L.; Nir, E.; Kabelac, M.; Hobza, P.; de Vries, M. S. *Proc. Natl. Acad. Sci. U.S.A.* **2005**, *102*, 20–23.
(12) Schultz, T.; Samoylova, E.; Radloff, W.; Hertel, I. V.; Sobolewski, A. L.; Domcke, W. *Science* **2004**, *306*, 1765–1768.
(13) Samoylova, E.; Smith, V. R.; Ritze, H.-H.; Radloff, W.; Kabelac, M.; Schultz, T. *J. Am. Chem. Soc.* **2006**, *128*, 15652–15656.
(14) Stert, V.; Radloff, W.; Schulz, C. P.; Hertel, I. V. *Eur. Phys. J. D* **1998**, *5*, 97–106.
(15) Ahlrichs, R.; Bär, M.; Häser, M.; Horn, H.; Kölmel, C. *Chem. Phys. Lett.* **1989**, *162*, 165.
(16) Werner, H.-J.; Knowles, P. J.; Lindh, R.; Manby, F. R.; Schütz, M.; Celani, P.; Korona, T.; Rauhut, G.; Amos, R. D.; Bernhardsson, A.; Berning, A.; Cooper, D. L.; Deegan, M. J. O.; Dobbyn, A. J.; Eckert, F.; Hampel, C.; Hetzer, G.; Lloyd, A. W.; McNicholas, S. J.; Meyer, W.; Mura, M. E.; Nicklass, A.; Palmieri, P.; Pitzer, R.; Schumann, U.; Stoll, H.; Stone, A. J.; Tarroni, R.; Thorsteinsson, T. *Molpro*, a package of ab initio programs, version 2006.1, 2006.
(17) Hättig, C.; Weigend, F. *J. Chem. Phys.* **2000**, *113*, 5154–5161.
(18) Celani, P.; Werner, H. J. *J. Chem. Phys.* **2000**, *112*, 5546–5557.
(19) Weigend, F.; Häser, M. *Theor. Chem. Acc.* **1997**, *97*, 331–340.
(20) Borst, D. R.; Roscioli, J. R.; Pratt, D. W. *J. Phys. Chem. A* **2002**, *106*, 4022–4027.
(21) Kim, B. J.; Thantu, N.; Weber, P. M. *J. Chem. Phys.* **1992**, *97*, 5384–5391.
(22) Lin, J. L.; Wu, R. H.; Tzeng, W. B. *Chem. Phys. Lett.* **2002**, *353*, 55–62.
(23) Baek, S. J.; Choi, K. W.; Choi, Y. S.; Kim, S. K. *J. Chem. Phys.* **2002**, *117*, 2131–2140.
(24) Kobayashi, T.; Nagakura, S. *J. Electron Spectrosc. Relat. Phenom.* **1974**, *4*, 207–212.
(25) Kydd, R. A.; Mills, I. M. *J. Mol. Spectrosc.* **1972**, *42*, 320.
(26) Ye, E. Y.; Bettens, R. P. A. *J. Mol. Spectrosc.* **2004**, *223*, 73–79.
(27) Hollas, J. M.; Musa, H.; Ridley, T. *J. Mol. Spectrosc.* **1984**, *104*, 89–106.
(28) Wu, R. H.; Brutschy, B. *J. Phys. Chem. A* **2004**, *108*, 9715–9720.
(29) Zhang, F.; Ai, Y. J.; Luo, Y.; Fang, W. H. *J. Chem. Phys.* **2009**, *130*, 144315.
(30) Spectra were measured for 274 nm excitation and 3-photon, 800 nm/2-photon, 400 nm/one-photon, and 200 nm ionization as well as for 250 nm excitation and 3-photon, 800 nm/2-photon, and 400 nm ionization.
(31) BE = 1 × (4.53 eV) + 2 × (3.10 eV)−EKE.
(32) Sobolewski, A., private communication.

JP903460B